

# Decentralized Connectivity Maintenance for Multi-robot Systems Under Motion and Sensing Uncertainties

Akshay Shetty, Timmy Hussain and Grace Gao  
*Stanford University*

## BIOGRAPHY

**Akshay Shetty** is a postdoc in the Department of Aeronautics and Astronautics at Stanford University. He obtained his Ph.D. in Aerospace Engineering from University of Illinois at Urbana-Champaign, and his B.Tech. in Aerospace Engineering from Indian Institute of Technology Bombay. His research interests include safe positioning and navigation of autonomous systems.

**Timmy Hussain** is an M.S Candidate in the Department of Aeronautics and Astronautics at Stanford University. He received his B.S in Aerospace Engineering from Massachusetts Institute of Technology. His research interests include the control and navigation of autonomous systems.

**Grace Gao** is an assistant professor in the Department of Aeronautics and Astronautics at Stanford University. Before joining Stanford University, she was an assistant professor at University of Illinois at Urbana-Champaign. She obtained her Ph.D. degree at Stanford University. Her research is on robust and secure positioning, navigation and timing with applications to manned and unmanned aerial vehicles, robotics, and power systems.

## ABSTRACT

Communication connectivity is desirable for safe and efficient operation of multi-robot systems. While decentralized algorithms for connectivity maintenance have been explored in recent literature, the majority of these works do not account for robot motion and sensing uncertainties. These uncertainties are inherent in practical robots and result in robots deviating from their desired positions which could potentially result in a loss of connectivity. In this paper we present a Decentralized Connectivity Maintenance algorithm accounting for robot motion and sensing Uncertainties (DCMU). We first propose a novel weighted graph definition for the multi-robot system that accounts for the aforementioned uncertainties along with realistic connectivity constraints such as line-of-sight connectivity and collision avoidance. Next we design a decentralized gradient-based controller for connectivity maintenance where we derive the gradients of our weighted graph edge weights required for computing the control. Finally, we perform multiple simulations to validate the connectivity maintenance performance of our DCMU algorithm under robot motion and sensing uncertainties and show an improvement compared to previous work.

## I. INTRODUCTION

Multi-robot systems are increasingly being used for various tasks such as exploration, target tracking, and search and rescue [Rizk et al., 2019; Cortés and Egerstedt, 2017]. One of the primary advantages of multi-robot systems is their ability to coordinate using inter-robot communication, which allows them to execute complex tasks in a safe and efficient manner [Alanwar et al., 2019; Bhamidipati and Gao, 2019; Park and Hutchinson, 2018]. Thus, it is highly desirable to maintain communication connectivity within the multi-robot system.

Existing literature has explored *decentralized* algorithms for connectivity maintenance due to their communication efficiency and scalability properties [Khateri et al., 2019]. These works typically represent the system as a weighted graph, where each node represents a robot and each edge represents the communication connection between two robots [Yang et al., 2010; Sabattini et al., 2013; Robuffo Giordano et al., 2013]. The edge weights between robots are formulated as a function of the robot positions subject to constraints such as maximum communication range, line-of-sight communication and collision avoidance (both inter-robot and obstacles). One commonly used metric for the connectivity of the system is algebraic connectivity, which depends on the graph edge weights as explained later in Section II. A value greater than zero indicates that the system is connected. Thus, in order to maintain connectivity within the system, previous works [Yang et al., 2010; Sabattini et al., 2013; Robuffo Giordano et al., 2013] derive a decentralized gradient-based controller to maintain the algebraic connectivity above a specified lower limit.

While previous works present efficient decentralized algorithms for connectivity maintenance, they assume that the robot positions are deterministic and do not explicitly account for robot motion and sensing uncertainties. Here, motion uncertainties

	Decentralized	Motion and sensing uncertainties	Line-of-sight and collision avoidance
[Yang et al., 2010][Sabattini et al., 2013] [Gasparrini et al., 2017][Siligardi et al., 2019]	✓		
[Robuffo Giordano et al., 2013]	✓		✓
[Shetty et al., 2020]		✓	
<b>This work</b>	✓	✓	✓

**Table 1:** Comparison of connectivity maintenance works in terms of their decentralized nature, explicit accounting of motion and sensing uncertainties, and considering realistic constraints such as line-of-sight communication and collision avoidance.

refer to the errors between the actual robot motion and a mathematical motion model, whereas sensing uncertainties refer to errors in measurements such as errors in localization measurements. These motion and sensing uncertainties, which are inherent in practical robots, result in robots deviating from their desired nominal positions. These deviations, if not accounted for, can potentially result in a loss of connectivity in the multi-robot system. Thus, it is important to account for robot motion and sensing uncertainties while designing connectivity maintenance algorithms.

In our prior work [Shetty et al., 2020] we define a weighted graph to represent the connectivity of the multi-robot system while accounting for deviations due to motion and sensing uncertainties. We then use a distributed trajectory planner to maintain connectivity within the system. However, our planner in [Shetty et al., 2020] requires a centralized communication setup, i.e., each robot communicates with all other robots in the system in a single planning iteration. While such communication is possible (perhaps via multi-hop connections), in practice it introduces additional communication delays and does not scale favorably to large systems. Thus, decentralized algorithms, as proposed in [Yang et al., 2010; Sabattini et al., 2013; Robuffo Giordano et al., 2013], are desirable since they require a robot to communicate only with its immediate neighboring robots in a single planning iteration. Additionally, the weighted graph in [Shetty et al., 2020] assumes a simplistic connectivity model subject to only a maximum communication range constraint, as opposed to the more realistic line-of-sight communication and collision avoidance constraints in [Robuffo Giordano et al., 2013].

In this work we present a decentralized algorithm (referred to as DCMU) for connectivity maintenance of multi-robot systems while accounting for motion and sensing uncertainties. A decentralized gradient-based controller is implemented in order to maintain system connectivity subject to constraints of maximum communication range, line-of-sight communication and collision avoidance. Table 1 outlines the contributions of this work in comparison to previous connectivity maintenance works. This paper is based on our work in [Shetty et al., 2021]. The main contributions of this work are listed as follows:

1. We propose a weighted graph that accounts for deviations in robot positions arising due to **motion and sensing uncertainties**. Compared to our prior work [Shetty et al., 2020], we include more realistic constraints of **line-of-sight** communication and **collision avoidance** (both inter-robot and obstacles) in addition to a maximum communication range.
2. Next, we derive a **decentralized gradient-based controller** in order to maintain the algebraic connectivity of the proposed weighted graph above a specified lower limit. Here we derive the gradients of the edge weights of our weighted graph that are required for computing the control. These edge weights account for deviations in robot positions instead of assuming deterministic robot positions as in [Yang et al., 2010; Sabattini et al., 2013].
3. Finally, we present extensive simulation results to evaluate our DCMU algorithm under motion and sensing uncertainties. We compare our connectivity maintenance performance with [Sabattini et al., 2013] and validate our algorithm on a high-fidelity simulator [Shah et al., 2018].

The remainder of the paper is organized as follows. We first introduce relevant background from graph theory in Section II. Next, in Section III we describe the models used for the robot motion and sensing uncertainties, and formulate the connectivity maintenance problem. Section IV provides details of our DCMU algorithm including the weighted graph definition and the gradient-based controller. Finally, in Section V we present simulation results validating the connectivity maintenance performance of our algorithm.

## II. PRELIMINARIES: GRAPH THEORY

A multi-robot system can be represented as an undirected graph, where each node represents a robot and each edge represents the communication connection between two robots. Let  $n$  be the number of nodes in the graph. The adjacency matrix  $A$  of the graph is defined as a  $n \times n$  matrix where  $a_{ij} \in [0, 1]$  represents the edge weight between two nodes  $i$  and  $j$ , with  $a_{ii} = 0$  [Grone et al., 1990]. The degree of a node is defined as  $d_i = \sum_{j=1}^n a_{ij}$ . The vector of node degrees  $\mathbf{d} = [d_1, \dots, d_n]$  is then used to define the degree matrix  $D$  of the graph as  $D = \text{diag}(\mathbf{d})$ . Given matrices  $A$  and  $D$  the Laplacian matrix  $L$  of the graph is

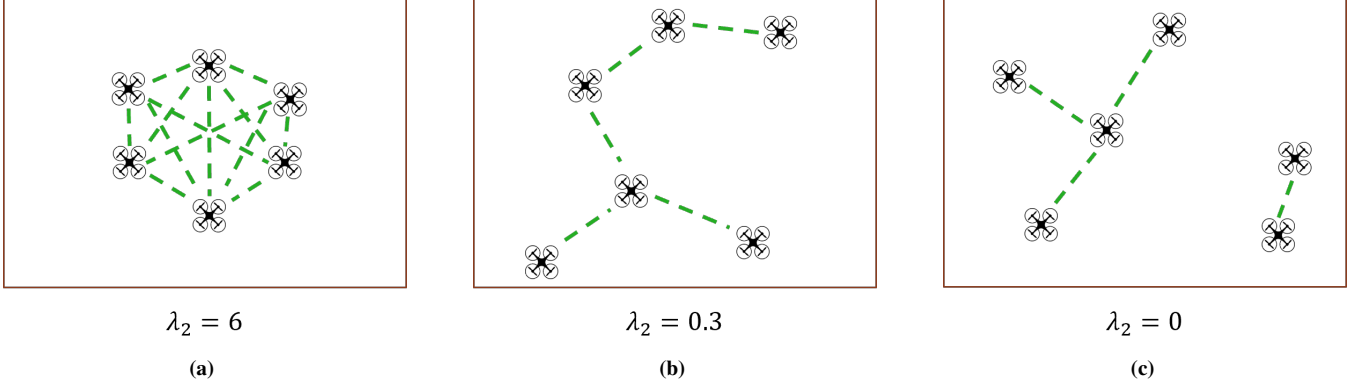


**Figure 1:** The algebraic connectivity  $\lambda_2$  of a graph varies from the number of nodes (fully-connected graph) to zero (disconnected graph).  $\lambda_2 > 0$  implies that the graph is connected.

defined as  $L = D - A$  [Grone et al., 1990].

Let  $\lambda_1 \leq \lambda_2 \leq \dots \leq \lambda_n$  be the eigenvalues of  $L$ . The algebraic connectivity of the graph, also known as the Fiedler value, is defined as the second-smallest eigenvalue of  $L$ , i.e.,  $\lambda_2$ . As mentioned in Section I, algebraic connectivity is a commonly used metric to represent the connectivity of multi-robot systems. It varies from zero (if the graph is disconnected) to the number nodes in the graph (if the graph is fully connected), i.e.  $0 \leq \lambda_2 \leq n$ . Fig. 1 illustrates the algebraic connectivity for different configurations of a graph. Thus,  $\lambda_2$  remains greater than 0 as long as there exists a (potentially multi-hop) communication path between any two robots in the system.

### III. PROBLEM FORMULATION

#### 1. Robot description

For each robot  $i$  in the multi-robot system, we consider a discrete-time single-integrator motion model:

$$\mathbf{x}_{i,t} = \mathbf{x}_{i,t-1} + B\mathbf{u}_{i,t-1} + \mathbf{w}_{i,t}, \quad (1)$$

where  $t$  represents the time instant,  $\mathbf{x}_{i,t}$  is the state vector representing the robot position,  $\mathbf{u}_{i,t}$  is the velocity control input,  $B$  is the control input matrix, and  $\mathbf{w}_{i,t}$  is a zero-mean Gaussian-distributed error vector with covariance matrix  $Q_{i,t}$ , i.e.,  $\mathbf{w}_{i,t} \sim \mathcal{N}(\mathbf{0}, Q_{i,t})$ . The control input matrix in Equation (1) is set as  $B = (\Delta t)I$ , where  $\Delta t$  is the discrete time-step. Note that while this is a simplified motion model, it can still be used to control real robots as demonstrated in previous works on ground and aerial robots [Soukieh et al., 2009; Lee et al., 2013]. For the sensing model, we assume each robot  $i$  obtains position measurements:

$$\mathbf{z}_{i,t} = \mathbf{x}_{i,t} + \mathbf{v}_{i,t}, \quad (2)$$

where  $\mathbf{z}_{i,t}$  is the measurement vector representing position measurements and  $\mathbf{v}_{i,t}$  is a zero-mean Gaussian-distributed error vector with covariance matrix  $R_{i,t}$ , i.e.,  $\mathbf{v}_{i,t} \sim \mathcal{N}(\mathbf{0}, R_{i,t})$ . Given the linear motion and sensing models with Gaussian uncertainties, we set each robot to use a Kalman Filter (KF) for state estimation. The prediction step of the KF is performed as:

$$\bar{\mathbf{x}}_{i,t} = \hat{\mathbf{x}}_{i,t-1} + B\mathbf{u}_{i,t-1}, \quad (3)$$

$$\bar{P}_{i,t} = P_{i,t-1} + Q_{i,t}, \quad (4)$$

where  $P_{i,t}$  is the state estimation covariance matrix such that  $\mathbf{x}_{i,t} \sim \mathcal{N}(\hat{\mathbf{x}}_{i,t}, P_{i,t})$ . The correction step of the KF is performed as:

$$G_{i,t} = \bar{P}_{i,t}(\bar{P}_{i,t} + R_{i,t})^{-1}, \quad (5)$$

$$\hat{\mathbf{x}}_{i,t} = \bar{\mathbf{x}}_{i,t} + G_{i,t}(\mathbf{z}_{i,t} - \bar{\mathbf{x}}_{i,t}), \quad (6)$$

$$P_{i,t} = \bar{P}_{i,t} - G_{i,t}\bar{P}_{i,t}, \quad (7)$$

where  $G_{i,t}$  is the Kalman gain matrix. In order to track a desired nominal state  $\check{\mathbf{x}}_{i,t}$ , we assume that each robot uses linear feedback control, where the total control input  $\mathbf{u}_{i,t}$  is of the form:

$$\mathbf{u}_{i,t} = \check{\mathbf{u}}_{i,t} - \check{K}_i(\hat{\mathbf{x}}_{i,t} - \check{\mathbf{x}}_{i,t}), \quad (8)$$

where  $\check{K}_i$  is the feedback control gain which can be designed using methods such as classical control theory or LQR design [Doyle et al., 2013], and  $\check{\mathbf{u}}_{i,t}$  is the nominal control input which relates to the nominal states as:

$$\check{\mathbf{x}}_{i,t} = \check{\mathbf{x}}_{i,t-1} + B\check{\mathbf{u}}_{i,t-1}. \quad (9)$$

Later in Section III.2 we discuss how the nominal control input is obtained for different robots in the multi-robot system.

Given the above setup for each robot  $i$ , the distribution of the robot's true state  $\mathbf{x}_{i,t}$  about its nominal state  $\check{\mathbf{x}}_{i,t}$  can be obtained using the method described in [Bry and Roy, 2011]. The authors derive the following Gaussian distribution for the robot's true state:

$$\mathbf{x}_{i,t} \sim \mathcal{N}(\check{\mathbf{x}}_{i,t}, \Sigma_{i,t}) \quad (10)$$

where  $\Sigma_{i,t} = P_{i,t} + \Lambda_{i,t}$ . Here  $P_{i,t}$  is the state estimation covariance matrix from Equation (7), and  $\Lambda_{i,t}$  can be obtained iteratively as follows [Bry and Roy, 2011]:

$$\Lambda_{i,t} = (I - B\check{K}_i)\Lambda_{i,t-1}(I - B\check{K}_i)^\top + G_{i,t}\bar{P}_{i,t}, \quad (11)$$

where  $I$  is an identity matrix and  $\Lambda_{i,0} = O$ . In essence, the distribution  $\mathbf{x}_{i,t} \sim \mathcal{N}(\check{\mathbf{x}}_{i,t}, \Sigma_{i,t})$  in Equation (10) captures the deviations of the robot's position from its desired nominal position that arise due to the motion and sensing uncertainties.

## 2. Multi-robot system: Connectivity maintenance

We consider the multi-robot system to be comprised of two types of robots: leader robots and follower robots. For the leader robots we assume that the nominal control inputs in Equation (9) are available from a high-level planner such as from an exploration or a search and rescue strategy [Burgard et al., 2005; Baxter et al., 2007]. On the other hand, the objective of follower robots is to maintain connectivity within the multi-robot system. Our DCMU algorithm presented in Section IV focuses on deriving the nominal control inputs for these follower robots.

In practice the communication connectivity between two robots can be considered to be binary, i.e., the robots are either connected if certain constraints are satisfied (such as minimum signal strength, bandwidth, etc.) or they are disconnected. We consider any two robots  $i$  and  $j$  in the multi-robot system to be connected if the following constraints are satisfied:

1. Communication range constraint: The distance between the robots is within a maximum communication range  $\rho$ , i.e.,  $\|\mathbf{x}_{i,t} - \mathbf{x}_{j,t}\|_2 \leq \rho$ .
2. Line-of-sight constraint: The robots maintain a direct line-of-sight, i.e., the line segment connecting  $\mathbf{x}_{i,t}$  and  $\mathbf{x}_{j,t}$  is not obstructed by obstacles in the environment.
3. Collision avoidance constraint: The robots are not colliding with any obstacles or other robots in the system. This constraint helps ensure that the communication equipment is not possibly damaged due a collision.

Let  $\bar{a}_{ij} = \{0, 1\}$  represent the binary connectivity between robots  $i$  and  $j$ , i.e.,  $\bar{a}_{ij} = 1$  if the robots are connected (the above constraints are satisfied) and  $\bar{a}_{ij} = 0$  otherwise (any of the above constraints is not satisfied). Note that by definition  $\bar{a}_{ii} = 0$ . These  $\bar{a}$  can then be used to obtain the algebraic connectivity  $\bar{\lambda}_2$  (as explained in Section II) of the graph which represents the connectivity of the multi-robot system based on the actual robot positions  $\mathbf{x}_{i,t}$ . Thus,  $\bar{\lambda}_2 > 0$  implies that the multi-robot system is connected.

We define the problem for our DCMU algorithm as: given a multi-robot system as described in this section, derive nominal control inputs ( $\check{\mathbf{u}}_{i,t}$  in Equation (9)) for the follower robots such that  $\bar{\lambda}_2$  is always above a specified lower limit  $\epsilon$ , i.e.,  $\bar{\lambda}_2 > \epsilon$ . Fig. 2 illustrates the defined problem.

## IV. PROPOSED CONNECTIVITY MAINTENANCE ALGORITHM: DCMU

During execution, each robot  $i$  in the multi-robot system deviates from its desired nominal position  $\check{\mathbf{x}}_{i,t}$  due to motion and sensing uncertainties. Previous connectivity maintenance works [Yang et al., 2010; Sabattini et al., 2013; Robuffo Giordano et al., 2013; Gasparri et al., 2017; Siligardi et al., 2019] that do not account for these uncertainties essentially assume that the

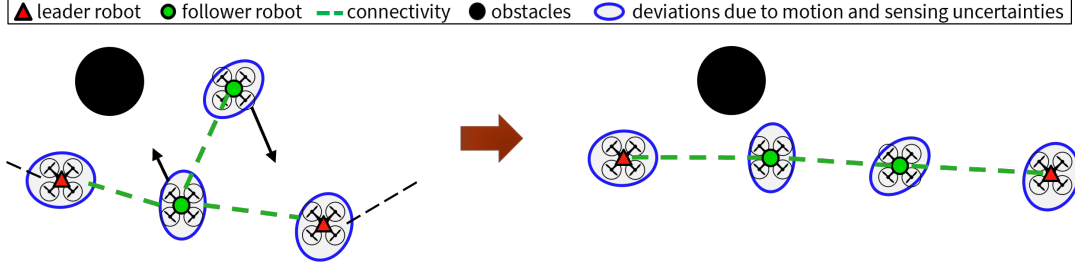


**Figure 2:** Illustration of the problem definition for our DCMU algorithm. Given a multi-robot system with leader robots and follower robots where the leader robots are controlled by some high-level planner (black-dashed lines), the objective of our DCMU algorithm is to derive nominal control inputs (black arrows) for the follower robots such that communication connectivity is maintained within the multi-robot system. Note that our algorithm must account for deviations in robot positions due to motion and sensing uncertainties.

robots are at their nominal positions, i.e.,  $\mathbf{x}_{i,t} = \check{\mathbf{x}}_{i,t}$ . In contrast, our DCMU algorithm accounts for the deviations of  $\mathbf{x}_{i,t}$  from  $\check{\mathbf{x}}_{i,t}$  as modeled by Equation (10).

In this section we provide the details of our DCMU algorithm. We first define a weighted graph to represent the connectivity of the multi-robot system where the edge weights account for deviations due to motion and sensing uncertainties. Next, we implement a decentralized power iteration method for each robot to estimate connectivity information of the weighted graph. Finally, each follower robot uses a gradient-based controller to obtain the nominal control input  $\check{\mathbf{u}}_{i,t}$  for maintaining connectivity of the weighted graph. Here we derive the expressions for the gradients of our weighted graph edge weights, which are required to compute the nominal control input  $\check{\mathbf{u}}_{i,t}$ . While for simplicity we drop the time notation in the remainder of this section, the nominal control input computed by our DCMU algorithm is applicable for all time instants  $t$ .

## 1. Weighted graph definition

For the edge weights to represent connectivity between robots, it needs to consider the communication constraints listed in Section III.2. Thus for our weighted graph, we define the edge weight between any two robots  $i$  and  $j$  as a product of four factors:

$$a_{ij} = \alpha_{ij}\beta_{ij}\gamma_i\gamma_j, \quad (12)$$

where  $\alpha_{ij}$  is a factor for the communication range constraint,  $\beta_{ij}$  is a factor for the line-of-sight constraint, and  $\gamma_i$  and  $\gamma_j$  are factors for the collision avoidance constraints of the two robots. Note that Equation (12) ensures that the edge weight  $a_{ij}$  is equal to 0 (i.e., robots  $i$  and  $j$  are not connected) if any of the factors  $\alpha_{ij}$ ,  $\beta_{ij}$ ,  $\gamma_i$  or  $\gamma_j$  is equal to 0 (happens when the corresponding constraint is not satisfied). Next, we define *smooth* functions for each of these factors which allows us to compute gradient-based control inputs as discussed later in Section IV.3.

1. Communication range factor  $\alpha_{ij}$ : This factor indicates how well robots  $i$  and  $j$  are connected in terms of being within a maximum communication range. We begin by defining a conservative measure  $\bar{l}_{ij}$  for the range between two robots while accounting for their deviations from their nominal positions up to a desired confidence level.  $\bar{l}_{ij}$  is defined as:

$$\bar{l}_{ij} = \|\check{\mathbf{x}}_i - \check{\mathbf{x}}_j\|_2 + s\sqrt{\bar{\lambda}^{\Sigma_i}} + s\sqrt{\bar{\lambda}^{\Sigma_j}}, \quad (13)$$

where  $\check{\mathbf{x}}_i$  and  $\check{\mathbf{x}}_j$  are the nominal positions,  $s$  is a scalar value reflecting a desired confidence level [Hoover, 1984], and  $\bar{\lambda}^{\Sigma_i}$  and  $\bar{\lambda}^{\Sigma_j}$  are the largest eigenvalues of the covariance matrices  $\Sigma_i$  and  $\Sigma_j$ . We have observed that a  $3\sigma$  confidence level results in acceptable connectivity maintenance performance. Fig. 3(a) illustrates the conservative measure  $\bar{l}_{ij}$ .

Given  $\bar{l}_{ij}$  and given a maximum communication range  $\rho$ , we define the communication range factor in Equation (12) as:

$$\alpha_{ij} = \begin{cases} 1 & 0 \leq \bar{l}_{ij} \leq \rho_0 \\ \frac{1}{2} + \frac{1}{2} \cos \left[ \frac{\pi(\bar{l}_{ij} - \rho_0)}{\rho - \rho_0} \right] & \rho_0 < \bar{l}_{ij} \leq \rho, \\ 0 & \bar{l}_{ij} > \rho \end{cases}, \quad (14)$$

where  $\rho_0$  is a parameter such that  $\rho_0 < \rho$ . Fig. 4(a) shows how  $\alpha_{ij}$  varies with  $\bar{l}_{ij}$ .

2. Line-of-sight range factor  $\beta_{ij}$ : This factor indicates how well robots  $i$  and  $j$  are connected in terms of being in line-of-sight of each other. Similar to  $\bar{l}_{ij}$  in Equation (13) we define a conservative measure  $\bar{l}_{ij,o}$  for how close the line-of-sight vector

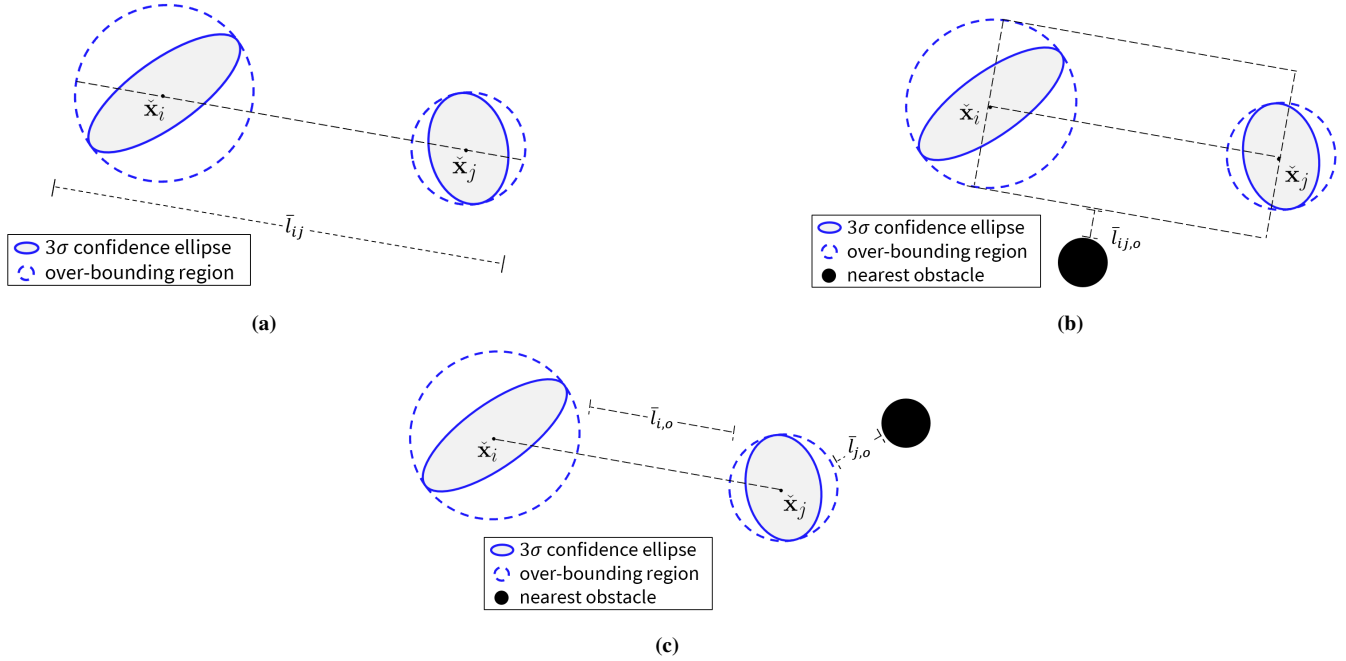


**Figure 3:** Conservative measures used to define our weighted graph in Section IV.1 that accounts for robot deviations due to motion and sensing uncertainties around their nominal positions  $\tilde{\mathbf{x}}_i$  and  $\tilde{\mathbf{x}}_j$ . (a)  $\bar{l}_{ij}$ : A conservative measure of the distance between two robots used for the communication range factor in Section IV.1.1. (b)  $\bar{l}_{ij,o}$ : A conservative measure of distance between the line-of-sight and the closest obstacle used for the line-of-sight factor in Section IV.1.2. (c)  $\bar{l}_{i,o}, \bar{l}_{j,o}$ : Conservative measures of the closest collision points for two robots. In this illustration the closest collision point for robot  $i$  is robot  $j$ , whereas for robot  $j$  it is the obstacle.

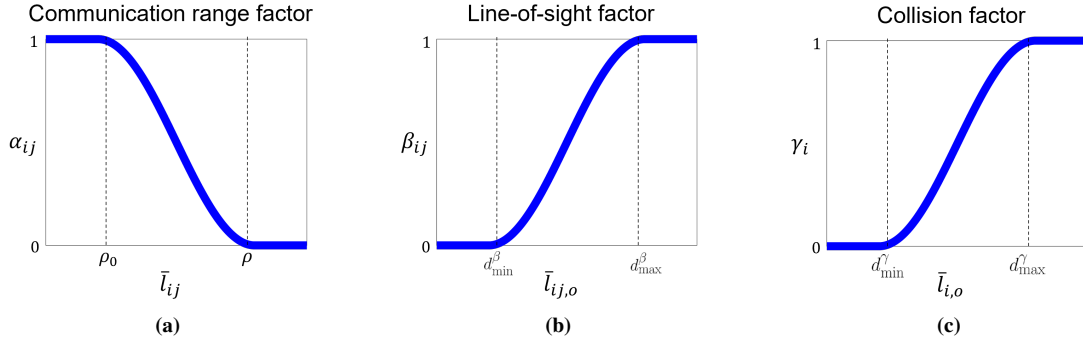


**Figure 4:** Factors that define the edge weights of our weighted graph using Equation (12). (a) Communication range factor (Equation (14)), (b) line-of-sight factor (Equation (17)), and (c) collision factor (Equation (19)).

between two robots is to nearby obstacles, as illustrated in Fig. 3(b). Thus,  $\bar{l}_{ij,o}$  is defined as:

$$\bar{l}_{ij,o} = \|\mathbf{x}_{l,ij} - \mathbf{x}_{\beta,ij}\|_2 - s\sqrt{\max(\bar{\lambda}^{\Sigma_i}, \bar{\lambda}^{\Sigma_j})}, \quad (15)$$

where  $\mathbf{x}_{\beta,ij}$  is the closest obstacle point,  $s$  is a scalar value reflecting the desired confidence level [Hoover, 1984] (similar to Equation (14)),  $\bar{\lambda}^{\Sigma_i}$  and  $\bar{\lambda}^{\Sigma_j}$  are the largest eigenvalues of the covariance matrices  $\Sigma_i$  and  $\Sigma_j$ , and  $\mathbf{x}_{l,ij}$  is the point on the line segment connecting  $\tilde{\mathbf{x}}_i$  and  $\tilde{\mathbf{x}}_j$  that is closest to  $\mathbf{x}_{\beta,ij}$ , and can be expressed as:

$$\mathbf{x}_{l,ij} = \zeta\tilde{\mathbf{x}}_i + (1 - \zeta)\tilde{\mathbf{x}}_j, \quad (16)$$

where  $\zeta \in [0, 1]$ . Given  $\bar{l}_{ij,o}$  and given parameters for the minimum and maximum desired distances ( $d_{min}^\beta$  and  $d_{max}^\beta$ )

from the obstacle, we define the line-of-sight factor in Equation (12) as:

$$\beta_{ij} = \begin{cases} 1 & \bar{l}_{ij,o} > d_{max}^\beta \\ \frac{1}{2} + \frac{1}{2} \cos \left[ \frac{\pi(d_{max}^\beta - \bar{l}_{ij,o})}{d_{max}^\beta - d_{min}^\beta} \right] & d_{min}^\beta < \bar{l}_{ij,o} \leq d_{max}^\beta \\ 0 & \bar{l}_{ij,o} \leq d_{min}^\beta \end{cases} \quad (17)$$

Fig. 4(b) shows how  $\beta_{ij}$  varies with  $\bar{l}_{ij,o}$ .

3. Collision factor  $\gamma_i$ : This factor indicates how close robot  $i$  is to a collision. Here again we define a conservative measure  $\bar{l}_{i,o}$  of the distance from the robot to the nearest possible collision point. This nearest collision point can be a neighboring robot or a nearby obstacle. Fig.3(c) illustrates the conservative measure for two robots  $i$  and  $j$ , i.e.,  $\bar{l}_{i,o}$  and  $\bar{l}_{j,o}$ . We define the measure  $\bar{l}_{i,o}$  as:

$$\bar{l}_{i,o} = \|\check{\mathbf{x}}_i - \mathbf{x}_{\gamma,i}\|_2 - s\sqrt{\lambda^{\Sigma_i}} - b_{i,o} \quad (18)$$

where  $\check{\mathbf{x}}_i$  is the nominal position and  $s$  is a scalar value reflecting the desired confidence level [Hoover, 1984] (similar to Equation (14)). Here if the nearest collision point for robot  $i$  is robot  $j$ , then  $\mathbf{x}_{\gamma,i} = \check{\mathbf{x}}_j$  and  $b_{i,o} = s\sqrt{\lambda^{\Sigma_j}}$ . Otherwise, if the nearest collision point for robot  $i$  is an obstacle then  $\mathbf{x}_{\gamma,i}$  is the center of the obstacle and  $b_{i,o}$  represents the width of the obstacle. Given  $\bar{l}_{i,o}$  and given parameters for the minimum and maximum desired distances ( $d_{min}^\gamma$  and  $d_{max}^\gamma$ ), we define the collision factor in Equation (12) as:

$$\gamma_i = \begin{cases} 1 & \bar{l}_{i,o} > d_{max}^\gamma \\ \frac{1}{2} + \frac{1}{2} \cos \left[ \frac{\pi(d_{max}^\gamma - \bar{l}_{i,o})}{d_{max}^\gamma - d_{min}^\gamma} \right] & d_{min}^\gamma < \bar{l}_{i,o} \leq d_{max}^\gamma \\ 0 & \bar{l}_{i,o} \leq d_{min}^\gamma \end{cases} \quad (19)$$

Fig. 4(c) shows how  $\gamma_i$  varies with  $\bar{l}_{i,o}$ . Note that similar to  $\gamma_i$ , the collision factor  $\gamma_j$  indicates how close robot  $j$  is to a collision.

Thus, given the nominal positions  $\check{\mathbf{x}}_i$  and covariance matrices  $\Sigma_i$  for all robots in the system, Equations (12)-(19) can be used to obtain the edge weights for our weighted graph. Note that since we use conservative measures in Equations (13), (15) and (18), our weighted graph is a conservative representation of the connectivity of the multi-robot system. Thus, our DCMU algorithm attempts to maintain the algebraic connectivity of our weighted graph  $\lambda_2 > \epsilon$  (as detailed later in Section IV.3) which results in maintaining the algebraic connectivity based on actual robot positions  $\lambda_2 > \epsilon$  (as shown later in Section V).

## 2. Decentralized power iteration

In order to compute the nominal control input for connectivity maintenance, each robot needs to obtain information of how well connected the weighted graph is. To obtain this information in a decentralized manner, we implement a decentralized power iteration method similar to previous works [Yang et al., 2010; Sabattini et al., 2013]. Here each robot  $i$  relies only on communicating with neighboring robots (other robots it is connected to) in a single planning iteration, and estimates the following two quantities:

1. The  $i^{th}$  component of the Fiedler vector (Section IV.1) of the weighted graph,  $\tilde{\mathbf{e}}_{2,i}^{(i)}$ . This contains information of how well robot  $i$  is connected to the system.
2. The algebraic connectivity (Section IV.1) of the weighted graph,  $\tilde{\lambda}_{2,i}$ . This contains information of how well connected the entire multi-robot system is.

For additional details of the decentralized power iteration method, we refer our readers to [Sabattini et al., 2013].

## 3. Decentralized gradient-based controller

As mentioned in Section III.2, the objective of the controller is to derive the nominal control input  $\check{\mathbf{u}}_{i,t}$  for each follower robot  $i$  to maintain the algebraic connectivity  $\lambda_2$  above a specified lower limit  $\epsilon$ . In order to achieve this, we instead maintain the algebraic connectivity of our weighted graph  $\lambda_2$  above  $\epsilon$ , which is a conservative representation of the multi-robot system connectivity as explained at the end of Section IV.1.

We use a similar approach as [Sabattini et al., 2013], where we first define a value function  $V$  that depends on algebraic connectivity of our weighted graph  $\lambda_2$ , and then design a gradient-based controller for the follower robots to increase  $\lambda_2$ . The

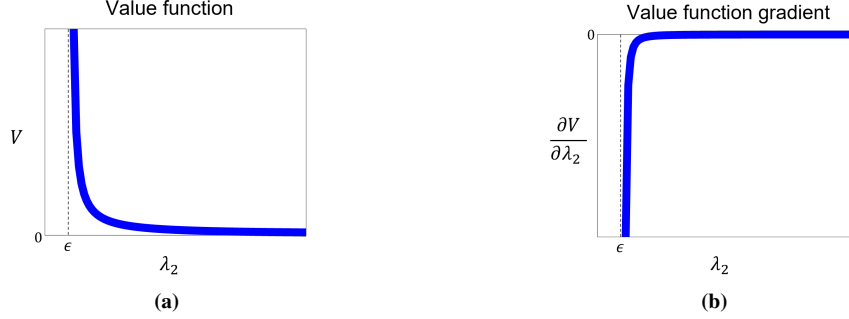


**Figure 5:** (a) The value function [Sabattini et al., 2013] defined in Equation (20), along with (b) the gradient of the value function required to compute the nominal control input in Equation (22).

value function is defined as:

$$V(\lambda_2) = \begin{cases} \coth(\lambda_2 - \epsilon) & \lambda_2 > \epsilon \\ 0 & \text{otherwise} \end{cases}. \quad (20)$$

Fig. 5(a) shows the variation of the value function with  $\lambda_2$ . In order to maintain connectivity, we seek to adjust the robots' nominal positions result in order to perform a gradient descent of the value function. This consequently results in increasing the value of  $\lambda_2$  as seen in Fig. 5(a). Thus, after simplification of the value function gradient [Yang et al., 2010; Sabattini et al., 2013], the desired change in the robot's nominal position can be expressed as:

$$\Delta \tilde{\mathbf{x}}_i = \left( -\frac{\partial V(\lambda_2)}{\partial \tilde{\mathbf{x}}_i} \right) = \left( -\frac{\partial V(\lambda_2)}{\partial \lambda_2} \right) \frac{\partial \lambda_2}{\partial \tilde{\mathbf{x}}_i} = \left( -\frac{\partial V(\lambda_2)}{\partial \lambda_2} \right) \sum_{j=1}^n \frac{\partial a_{ij}}{\partial \tilde{\mathbf{x}}_i} \left( \tilde{\mathbf{e}}_{2,i}^{(i)} - \tilde{\mathbf{e}}_{2,j}^{(j)} \right)^2, \quad (21)$$

where the gradient of the value function  $\frac{\partial V(\lambda_2)}{\partial \lambda_2}$  is evaluated at  $\tilde{\lambda}_{2,i}$ . Here  $\tilde{\lambda}_{2,i}$ ,  $\tilde{\mathbf{e}}_{2,i}^{(i)}$  and  $\tilde{\mathbf{e}}_{2,j}^{(j)}$  are obtained from the decentralized power iteration method as explained in Section IV.2. Fig. 5(b) shows the gradient of the value function. Note that as  $\lambda_2$  approaches  $\epsilon$ , the magnitude of the gradient sharply increases resulting in a large  $\Delta \tilde{\mathbf{x}}_i$ . This consequently leads to the follower robots moving faster (limited by their maximum velocity) to maintain connectivity when  $\lambda_2$  approaches  $\epsilon$ .

Thus, using Equations (9) and (21), the nominal control input can be obtained as:

$$\tilde{\mathbf{u}}_i = B^{-1} \Delta \tilde{\mathbf{x}}_i = \frac{1}{\Delta t} \left( -\frac{\partial V(\lambda_2)}{\partial \lambda_2} \right) \sum_{j=1}^n \frac{\partial a_{ij}}{\partial \tilde{\mathbf{x}}_i} \left( \tilde{\mathbf{e}}_{2,i}^{(i)} - \tilde{\mathbf{e}}_{2,j}^{(j)} \right)^2, \quad (22)$$

where note that the control input matrix  $B = (\Delta t)I$  from Equation (1).

In order to compute the nominal control input  $\tilde{\mathbf{u}}_i$  using the above equation, we require the gradients of the edge weights  $a_{ij}$  with respect to the robot nominal position  $\tilde{\mathbf{x}}_i$ , i.e.,  $\frac{\partial a_{ij}}{\partial \tilde{\mathbf{x}}_i}$ . Given the definition of the edge weight in Equation (12), the required gradient can be expressed as:

$$\frac{\partial a_{ij}}{\partial \tilde{\mathbf{x}}_i} = \frac{\partial \alpha_{ij}}{\partial \tilde{\mathbf{x}}_i} \beta_{ij} \gamma_i \gamma_j + \alpha_{ij} \frac{\partial \beta_{ij}}{\partial \tilde{\mathbf{x}}_i} \gamma_i \gamma_j + \alpha_{ij} \beta_{ij} \frac{\partial \gamma_i}{\partial \tilde{\mathbf{x}}_i} \gamma_j + \alpha_{ij} \beta_{ij} \gamma_i \frac{\partial \gamma_j}{\partial \tilde{\mathbf{x}}_i}. \quad (23)$$

In the remainder of this subsection we proceed to derive the expressions for the gradient of the factors  $\alpha_{ij}$ ,  $\beta_{ij}$ ,  $\gamma_i$  and  $\gamma_j$  with respect to  $\tilde{\mathbf{x}}_i$ . From Equation (14), the gradient of  $\alpha_{ij}$  can be expressed as:

$$\frac{\partial \alpha_{ij}}{\partial \tilde{\mathbf{x}}_i} = -\frac{\pi}{2(\rho - \rho_0)} \sin \left[ \frac{\pi(\bar{l}_{ij} - \rho_0)}{\rho - \rho_0} \right] \frac{\partial \bar{l}_{ij}}{\partial \tilde{\mathbf{x}}_i}, \quad (24)$$

where using Equation (13), the gradient of  $\bar{l}_{ij}$  with respect to the  $m^{\text{th}}$  element of  $\tilde{\mathbf{x}}_i$  is:

$$\frac{\partial \bar{l}_{ij}}{\partial \tilde{\mathbf{x}}_i^{(m)}} = \frac{\tilde{\mathbf{x}}_i^{(m)} - \tilde{\mathbf{x}}_j^{(m)}}{\|\tilde{\mathbf{x}}_i - \tilde{\mathbf{x}}_j\|_2} + \frac{s}{2\sqrt{\lambda^{\Sigma_i}}} \frac{\partial \bar{\lambda}^{\Sigma_i}}{\partial \tilde{\mathbf{x}}_i^{(m)}}. \quad (25)$$



Next, for the gradient of  $\beta_{ij}$ , using Equation (17) we get:

$$\frac{\partial \beta_{ij}}{\partial \tilde{\mathbf{x}}_i} = \frac{\pi}{2(d_{max}^\beta - d_{min}^\beta)} \sin \left[ \frac{\pi(d_{max}^\beta - \bar{l}_{ij,o})}{d_{max}^\beta - d_{min}^\beta} \right] \frac{\partial \bar{l}_{ij,o}}{\partial \tilde{\mathbf{x}}_i}, \quad (26)$$

where using Equation (15) the gradient of  $\bar{l}_{ij,o}$  with respect to the  $m^{th}$  element of  $\tilde{\mathbf{x}}_i$  is:

$$\frac{\partial \bar{l}_{ij,o}}{\partial \tilde{\mathbf{x}}_i^{(m)}} = \zeta \frac{(\tilde{\mathbf{x}}_i^{(m)} - \mathbf{x}_o^{(m)})}{\|\tilde{\mathbf{x}}_i - \mathbf{x}_o\|_2} - \frac{s}{2\sqrt{\max(\bar{\lambda}^{\Sigma_i}, \bar{\lambda}^{\Sigma_j})}} \frac{\partial \max(\bar{\lambda}^{\Sigma_i}, \bar{\lambda}^{\Sigma_j})}{\partial \tilde{\mathbf{x}}_i^{(m)}}. \quad (27)$$

Using Equation (19), the gradient of  $\gamma_i$  can be expressed as:

$$\frac{\partial \gamma_i}{\partial \tilde{\mathbf{x}}_i} = \frac{\pi}{2(d_{max}^\gamma - d_{min}^\gamma)} \sin \left[ \frac{\pi(d_{max}^\gamma - \bar{l}_{i,o})}{d_{max}^\gamma - d_{min}^\gamma} \right] \frac{\partial \bar{l}_{i,o}}{\partial \tilde{\mathbf{x}}_i}, \quad (28)$$

where using Equation (18) the gradient of  $\bar{l}_{i,o}$  with respect to the  $m^{th}$  element of  $\tilde{\mathbf{x}}_i$  is:

$$\frac{\partial \bar{l}_{i,o}}{\partial \tilde{\mathbf{x}}_i^{(m)}} = \frac{(\tilde{\mathbf{x}}_i^{(m)} - \mathbf{x}_o^{(m)})}{\|\tilde{\mathbf{x}}_i - \mathbf{x}_o\|_2} - \frac{s}{2\sqrt{\bar{\lambda}^{\Sigma_i}}} \frac{\partial \bar{\lambda}^{\Sigma_i}}{\partial \tilde{\mathbf{x}}_i^{(m)}}. \quad (29)$$

Since  $\gamma_j$  indicates how close robot  $j$  is to a collision, its gradient with respect to  $\tilde{\mathbf{x}}_i$  is non-zero only when the closest collision point for robot  $j$  is robot  $i$ . As explained below Equation (18), this implies  $\mathbf{x}_{\gamma_j} = \tilde{\mathbf{x}}_i$  and  $b_{j,o} = s\sqrt{\bar{\lambda}^{\Sigma_i}}$ . Thus, if the closest collision point for robot  $j$  is robot  $i$ , then using Equation (19) the gradient of  $\gamma_j$  can be expressed as:

$$\frac{\partial \gamma_j}{\partial \tilde{\mathbf{x}}_i} = \frac{\pi}{2(d_{max}^\gamma - d_{min}^\gamma)} \sin \left[ \frac{\pi(d_{max}^\gamma - \bar{l}_{j,o})}{d_{max}^\gamma - d_{min}^\gamma} \right] \frac{\partial \bar{l}_{j,o}}{\partial \tilde{\mathbf{x}}_i}, \quad (30)$$

where using Equation (18) the gradient of  $\bar{l}_{j,o}$  with respect to the  $m^{th}$  element of  $\tilde{\mathbf{x}}_i$  is:

$$\frac{\partial \bar{l}_{j,o}}{\partial \tilde{\mathbf{x}}_i^{(m)}} = -\frac{(\tilde{\mathbf{x}}_j^{(m)} - \tilde{\mathbf{x}}_i^{(m)})}{\|\tilde{\mathbf{x}}_j - \tilde{\mathbf{x}}_i\|_2} - \frac{s}{2\sqrt{\bar{\lambda}^{\Sigma_i}}} \frac{\partial \bar{\lambda}^{\Sigma_i}}{\partial \tilde{\mathbf{x}}_i^{(m)}}. \quad (31)$$

In order to compute the gradients of the factors using Equations (24), (26), (28) and (30), we need to derive the gradients of the eigenvalues of covariance matrices  $\Sigma_i$  and  $\Sigma_j$  required in Equations (25), (27), (29) and (31). The equations in Section III.1 show how the covariance matrix  $\Sigma_i$  for a robot varies with its position  $\tilde{\mathbf{x}}_i$ . From Equation (10), note that  $\Sigma_i = P_i + \Lambda_i$ . Thus, as the robot nominal position  $\tilde{\mathbf{x}}_i$  changes from time instant  $t$  to  $t+1$ , the covariance matrix updates to  $\Sigma_{i,t+1}$  as:

$$\Sigma_{i,t+1} = P_{i,t+1} + \Lambda_{i,t+1} \quad (32)$$

$$= \bar{P}_{i,t+1} - G_{i,t+1} \bar{P}_{i,t+1} + (I - BK_{i,t+1}) \Lambda_{i,t} (I - BK_{i,t+1})^\top + G_{i,t+1} \bar{P}_{i,t+1} \quad (33)$$

$$= P_{i,t} + Q_{i,t+1} + (I - BK_{i,t+1}) \Lambda_{i,t} (I - BK_{i,t+1})^\top. \quad (34)$$

Note that the updated covariance matrix  $\Sigma_{i,t+1}$  only depends on  $P_{i,t}$ ,  $Q_{i,t+1}$ ,  $B$ ,  $K_{i,t+1}$  and  $\Lambda_{i,t}$ , and does not depend on the new nominal position  $\tilde{\mathbf{x}}_{i,t+1}$ . Consequently, the eigenvalue  $\bar{\lambda}^{\Sigma_i}$  also does not depend on  $\tilde{\mathbf{x}}_i$ , which implies  $\frac{\partial \bar{\lambda}^{\Sigma_i}}{\partial \tilde{\mathbf{x}}_i^{(m)}} = 0$ . Thus, the terms involving gradients of the eigenvalues in Equations (25), (27), (29) and (31) are equal to zero.

In summary, our DCMU algorithm obtains the nominal control inputs  $\tilde{\mathbf{u}}_i$  for the follower robots using Equation (22), which relies on quantities estimated using the decentralized power iteration method mentioned in Section IV.2 and relies on gradients of our weighted graph edge weights described in Section IV.1. Equations (23)-(32) provide the details of how to compute these gradients.

## V. SIMULATION RESULTS

In this next section we validate the connectivity maintenance performance of our DCMU algorithm in two 2-dimensional simulation setups: MATLAB and AirSim [Shah et al., 2018]. We first present the MATLAB simulations which allow us to quantitatively compare our algorithm with related previous work in [Sabattini et al., 2013], which we refer to as the Sabattini algorithm for simplicity. We then discuss the AirSim simulations which validate our algorithm on a high-fidelity simulator. For both simulation setups we first demonstrate our DCMU algorithm on a simple two robot setup with one leader robot and one follower robot, and then proceed to more complex multi-robot configurations. The leader robots are given predefined nominal trajectories (which we assume are available from some high-level planner such as an exploration strategy), and the follower robots implement nominal control inputs from our DCMU algorithm, i.e., from Equation (22). A video containing the simulation results can be viewed online at [https://youtu.be/SbE-ejQ\\_zm8](https://youtu.be/SbE-ejQ_zm8).

For both our simulation setups we set the time-step  $\Delta t = 0.2$  s. The motion and sensing model error covariance matrices are set as  $Q_{i,t} = (0.02 \text{ m}^2)I$  and  $R_{i,t} = (5 \text{ m}^2)I$  respectively, and the initial state estimation covariance matrix is set as  $P_{i,t} = (0.1 \text{ m}^2)I$ . We set the control feedback gain used in Equation (8) as  $\tilde{K}_i = (0.14)I$ . For a  $3\sigma$  confidence level in our weighted graph, we obtain the scalar value  $s = 3.494$ . The communication range parameters in Equation (14) are set as  $\rho = 20$  m and  $\rho_0 = 18$  m. For the line-of-sight factor (Equation (17)) and the collision factor (Equation (19)) we set the parameters  $d_{max}^\beta = 3$  m,  $d_{min}^\beta = 1$  m,  $d_{max}^\gamma = 3$  m and  $d_{min}^\gamma = 1$  m. We limit the maximum speed of the robots to be  $2 \text{ m s}^{-1}$ , in order to reflect physical constraints of practical robots. Finally, we specify the lower limit for the algebraic connectivity of the system to be  $\epsilon = 0.01$ , where the connectivity maintenance objective is to maintain  $\bar{\lambda}_2 > \epsilon$ .

### 1. MATLAB simulations

For the MATLAB simulations, our primary objective is to compare the connectivity maintenance performance of our algorithm with the Sabattini algorithm [Sabattini et al., 2013] for various multi-robot system configurations. As mentioned in the beginning of Section IV, previous works [Yang et al., 2010; Sabattini et al., 2013; Robuffo Giordano et al., 2013; Gasparri et al., 2017; Siligardi et al., 2019] in essence assume that the robots are at their desired nominal positions. In contrast, our DCMU algorithm accounts for the deviations arising due to motion and sensing uncertainties.

As shown in Fig. 6, we first analyze a simple two robot setup with one leader robot and one follower. Fig. 6(a)-(d) show snapshots of a single simulation run where the follower robot implements our DCMU algorithm to maintain connectivity with

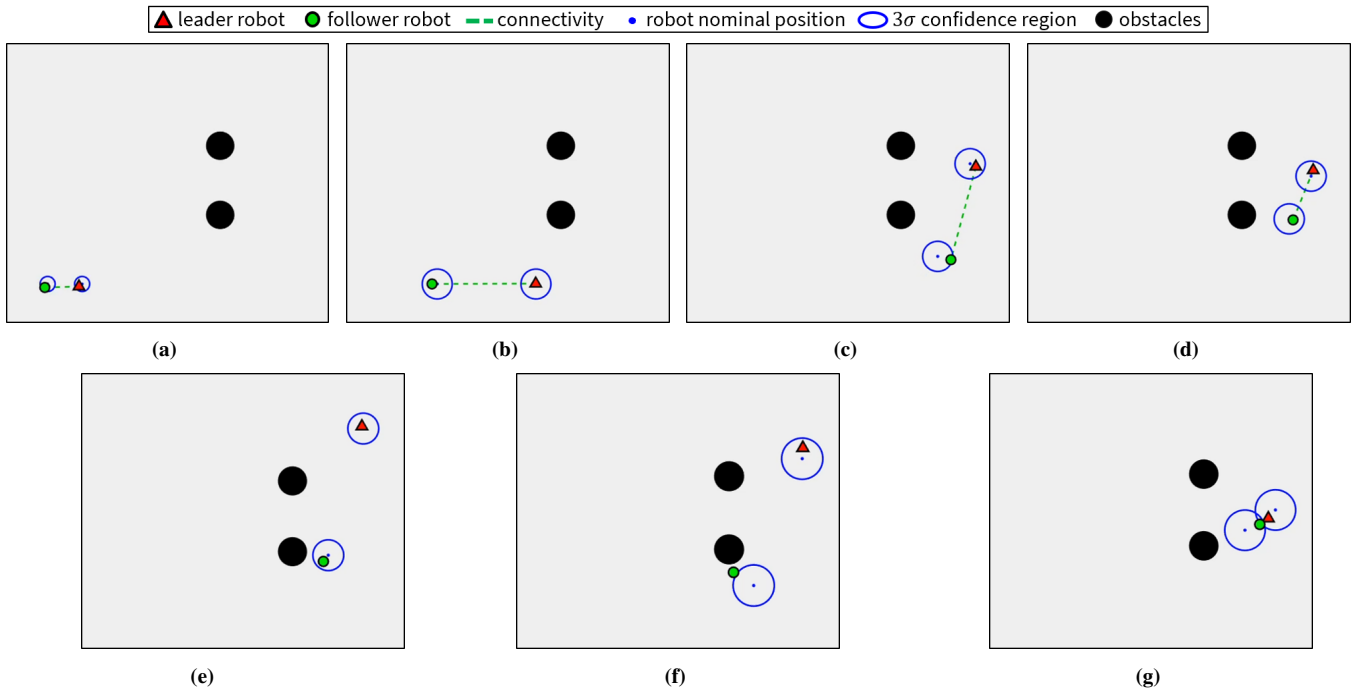


**Figure 6:** MATLAB simulation for a two-robot system. (a)-(d) Snapshots of a simulation run where the follower robot implements our DCMU algorithm. (e)-(g) Snapshots of different simulation runs where connectivity is lost when the follower robot implements the Sabattini algorithm [Sabattini et al., 2013].

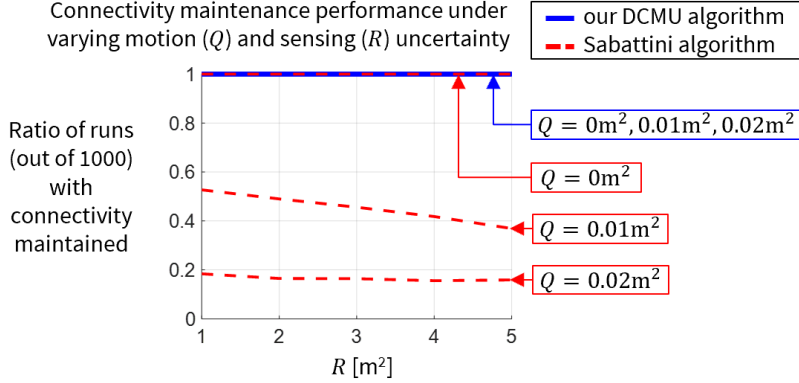


**Figure 7:** Quantitative comparison for the two-robot MATLAB simulation shown in Fig 6. Our DCMU algorithm performs better than the Sabattini [Sabattini et al., 2013] algorithm under increasing motion and sensing uncertainties.

the leader robot. Starting from an initial position (Fig. 6(a)), the follower robot follows the leader robot to stay within the communication range (Fig. 6(b)). As the leader robot moves upwards, the follower robot maintains line-of-sight connectivity while maintaining a safe distance from the obstacles (Fig. 6(c)), while also maintaining a safe distance from the leader robot itself (Fig. 6(d)). Fig. 6(e)-(g) show snapshots of different simulation runs where the follower robot implements the Sabattini algorithm, i.e. does not account for the motion and sensing uncertainties [Sabattini et al., 2013]. We observe that not accounting for these uncertainties can potentially lead to a loss of connection due to the robots getting further away than the communication range (Fig. 6(e)), or due to the robots losing line-of-sight communication (Fig. 6(f)), or due to a collision (Fig. 6(g)).

In Fig. 7, we provide a quantitative comparison with the Sabattini algorithm [Sabattini et al., 2013]. Here we vary the amount of motion and sensing uncertainties in the multi-robot system and perform 1000 simulation runs for each scenario for both our DCMU algorithm and the Sabattini algorithm. For both these algorithms we compare the ratio of runs for which the algebraic connectivity based on the actual robot positions  $\bar{\lambda}_2$  was maintained above the specified lower limit  $\epsilon = 0.01$ , as stated in the problem formulation in Section III. We observe that our DCMU algorithm maintains  $\bar{\lambda}_2 > \epsilon$  for all 1000 runs for the different motion and sensing uncertainties. The Sabattini algorithm performs similar to our algorithm when there are no motion and sensing uncertainties, i.e., when  $Q_{i,t} = (0 \text{ m}^2)I$  and  $R_{i,t} = (0 \text{ m}^2)I$  for all robots  $i$ . However, as the amount of uncertainty is increased, we observe that the ratio of runs for which the Sabattini algorithm maintains  $\bar{\lambda}_2 > \epsilon$  decreases sharply.

We then compare our algorithm with the Sabattini algorithm on different multi-robot system configurations as shown in Fig. 8. Snapshots of a single simulation run with follower robots using our DCMU algorithm are shown for three different configurations: Fig. 8(a)-(c), Fig. 8(d)-(f) and Fig. 8(g)-(i). Here we observe that the follower robots rearrange themselves in order to maintain connectivity within the system while accounting for the deviations arising due to motion and sensing uncertainties. Fig. 9 quantitatively compares the connectivity maintenance performance of our DCMU algorithm and the Sabattini algorithm for 1000 simulation runs of each of the three multi-robot configurations. Similar to the two-robot case, we observe that our algorithm maintains  $\bar{\lambda}_2 > \epsilon$  for all 1000 runs, whereas the ratio of runs for which Sabattini algorithm maintains  $\bar{\lambda}_2 > \epsilon$  sharply decreases as the amount of motion and sensing uncertainties increase. These simulations validate the applicability of our algorithm towards maintaining connectivity in the system under robot motion and sensing uncertainties.

## 2. AirSim simulations

For the AirSim simulations, we validate our algorithm on multi-robot systems comprising unmanned aerial vehicles (UAVs). The motion of the UAVs is modeled using Equation (1), while sensing uncertainties are introduced according to Equation (2). We show snapshots with the follower UAVs using our DCMU algorithm for three different configurations: Fig. 10(a)-(c), Fig. 10(d)-(f) and Fig. 10(g)-(i). In these snapshots we observe that as the leader UAVs follow their predefined nominal trajectories, the follower UAVs move to maintain connectivity within the system. Fig. 11 shows how the algebraic connectivity  $\bar{\lambda}_2$  is maintained above the lower limit  $\epsilon$  throughout the simulation for the different configurations. Note that the AirSim simulations are executed in *real-time*, thus validating the real-time applicability of our DCMU algorithm.

## VI. CONCLUSION

In this paper we presented a Decentralized Connectivity Maintenance algorithm that accounted for robot motion and sensing Uncertainties (DCMU). We first defined a weighted graph to account for these uncertainties along with constraints such as a maximum communication range, line-of-sight communication and collision avoidance. Next, we designed a decentralized

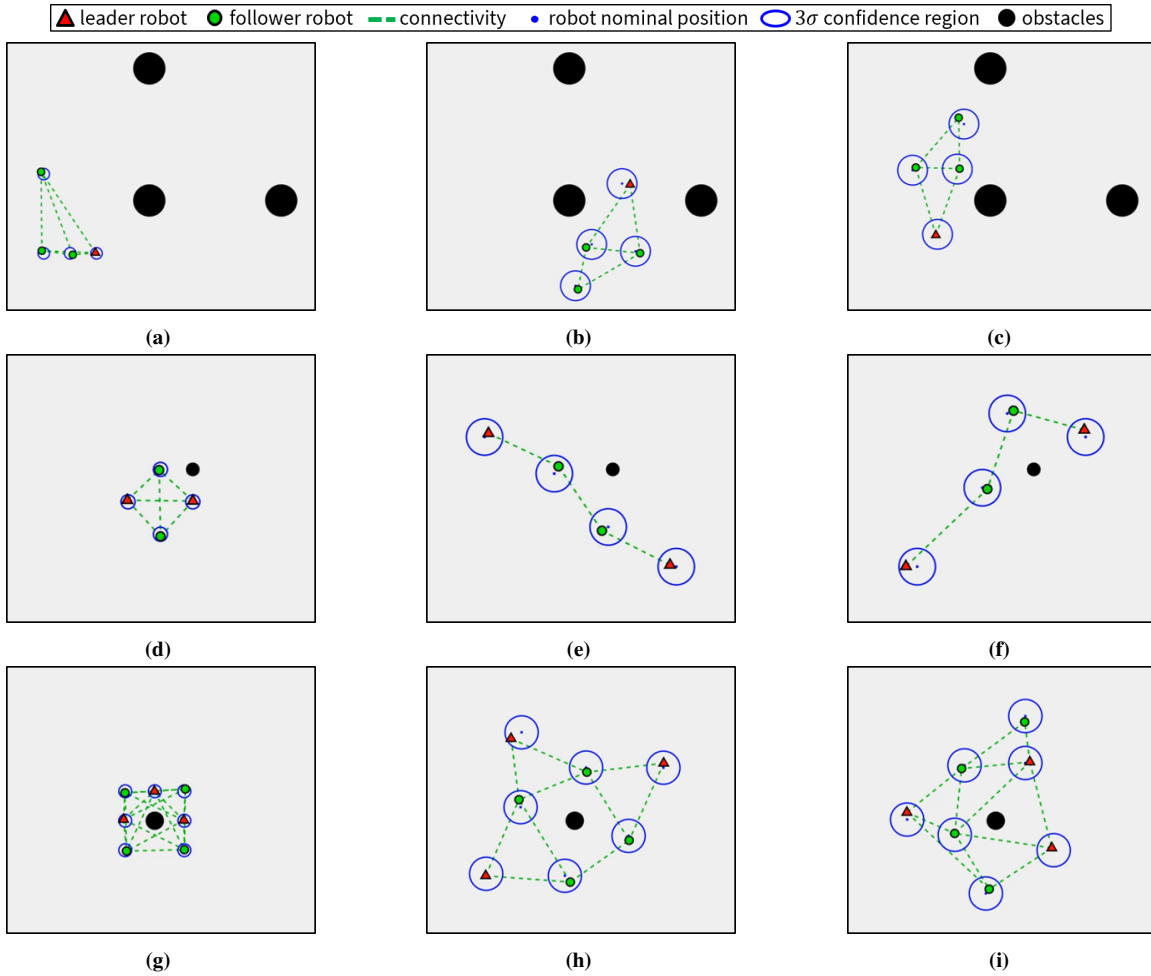


**Figure 8:** MATLAB simulations for various multi-robot system configurations. Snapshots of simulation runs where the follower robots implement our DCMU algorithm in three different configurations:(a)-(c), (d)-(f) and (g)-(i).

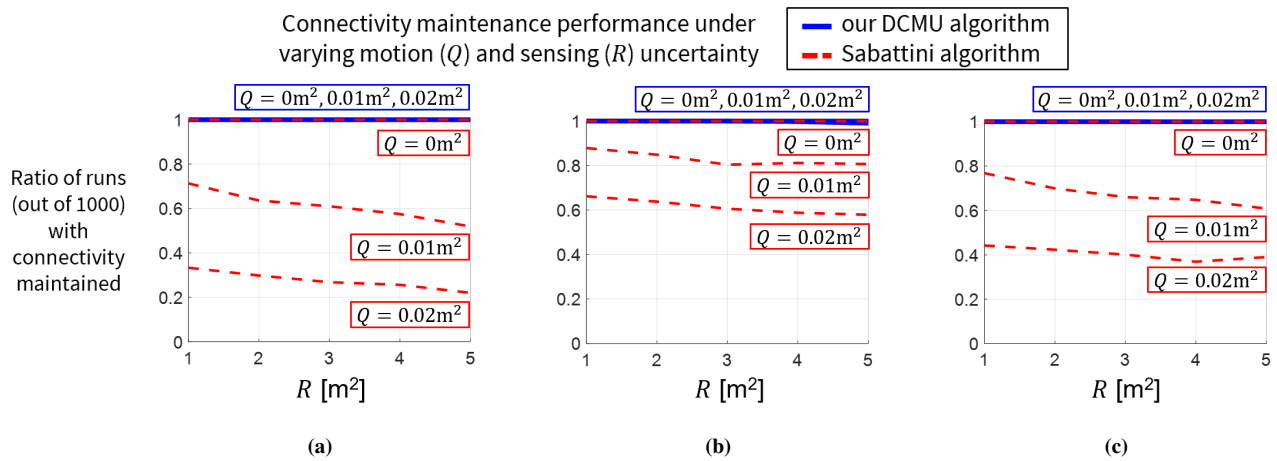


**Figure 9:** Quantitative comparisons for the multi-robot MATLAB simulations shown in Fig 8. Our DCMU algorithm performs better than the Sabattini algorithm [Sabattini et al., 2013] under increasing motion and sensing uncertainties for the three multi-robot configurations.

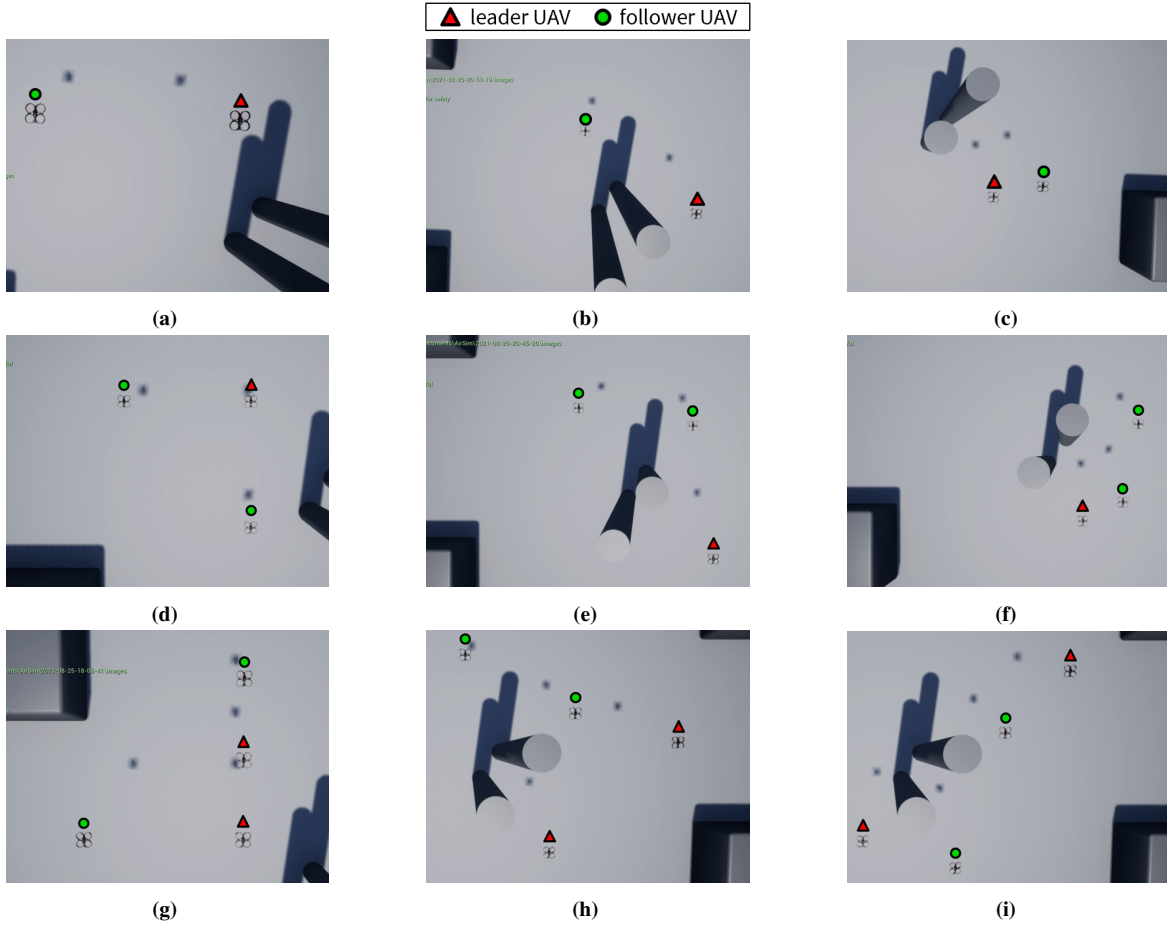


**Figure 10:** AirSim simulations for various multi-UAV system configurations. Snapshots of simulation runs where the follower UAVs implement our DCMU algorithm in three different configurations:(a)-(c), (d)-(f) and (g)-(i).

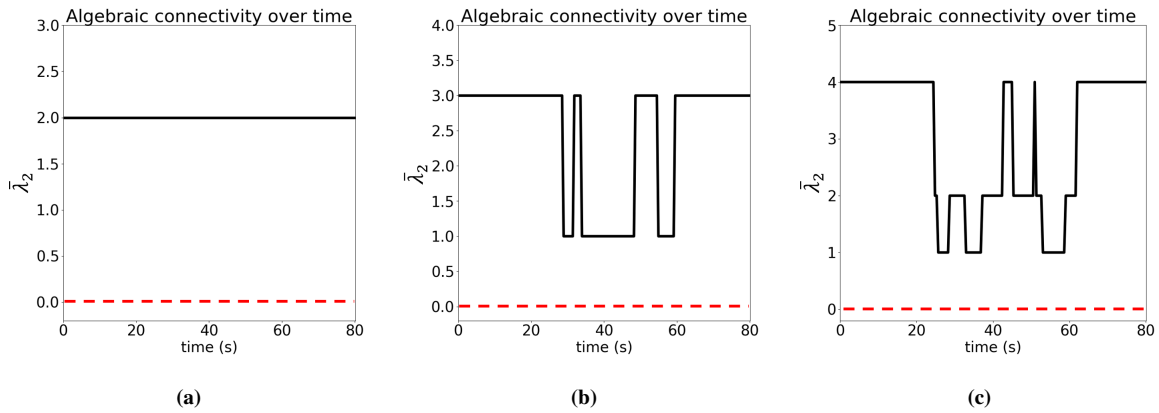


**Figure 11:** Algebraic connectivity of the multi-UAV AirSim simulations shown in Fig. 10. Our DCMU algorithm maintains  $\bar{\lambda}_2$  (black lines) above the lower limit  $\epsilon$  (red-dashed lines).

gradient-based controller by deriving the gradients of our weighted graph edge weights. Finally, we validated the connectivity maintenance performance of our algorithm on two simulation setups: MATLAB and AirSim. We quantitatively compared our DCMU algorithm with previous related work [Sabattini et al., 2013] and demonstrated that our algorithm performed better under motion and sensing uncertainties. Additionally, we also demonstrated the connectivity maintenance performance of our

algorithm on AirSim, which is a higher-fidelity simulator compared to MATLAB. Possible directions for future work include exploring alternate geometric representations that reduce the conservatism in our weighted graph, accounting for more complex robot motion and sensing models, and evaluating our DCMU algorithm on real hardware.

## REFERENCES

- Alanwar, A., Said, H., and Althoff, M. (2019). Distributed Secure State Estimation Using Diffusion Kalman Filters and Reachability Analysis. In *IEEE 58th Conference on Decision and Control (CDC)*, pages 4133–4139. IEEE. <https://doi.org/10.1109/CDC40024.2019.9029929>.
- Baxter, J. L., Burke, E., Garibaldi, J. M., and Norman, M. (2007). Multi-robot Search and Rescue: A Potential Field Based Approach. In *Autonomous Robots and Agents*, pages 9–16. Springer. [https://doi.org/10.1007/978-3-540-73424-6\\_2](https://doi.org/10.1007/978-3-540-73424-6_2).
- Bhamidipati, S. and Gao, G. X. (2019). Locating Multiple GPS Jammers Using Networked UAVs. *IEEE Internet of Things Journal*, 6(2):1816–1828. <https://doi.org/10.1109/JIOT.2019.2896262>.
- Bry, A. and Roy, N. (2011). Rapidly-Exploring Random Belief Trees for Motion Planning Under Uncertainty. In *IEEE international conference on robotics and automation*, pages 723–730. IEEE. <http://dx.doi.org/10.1109/ICRA.2011.5980508>.
- Burgard, W., Moors, M., Stachniss, C., and Schneider, F. E. (2005). Coordinated Multi-robot Exploration. *IEEE Transactions on Robotics*, 21(3):376–386. <https://doi.org/10.1109/TRO.2004.839232>.
- Cortés, J. and Egerstedt, M. (2017). Coordinated Control of Multi-robot Systems: A Survey. *SICE Journal of Control, Measurement, and System Integration*, 10(6):495–503.
- Doyle, J. C., Francis, B. A., and Tannenbaum, A. R. (2013). *Feedback Control Theory*. Courier Corporation. [http://dx.doi.org/10.1007/978-0-387-85460-1\\_1](http://dx.doi.org/10.1007/978-0-387-85460-1_1).
- Gasparri, A., Sabattini, L., and Ulivi, G. (2017). Bounded Control Law for Global Connectivity Maintenance in Cooperative Multirobot Systems. *IEEE Transactions on Robotics*, 33(3):700–717. <https://doi.org/10.1109/TRO.2017.2664883>.
- Grone, R., Merris, R., and Sunder, V. S. (1990). The Laplacian Spectrum of a Graph. *SIAM Journal on Matrix Analysis and Applications*, 11(2):218–238. <https://doi.org/10.1016/j.camwa.2004.05.005>.
- Hoover, W. E. (1984). Algorithms for Confidence Circles and Ellipses. *NOAA Technical Report*.
- Khateri, K., Pourgholi, M., Montazeri, M., and Sabattini, L. (2019). A Comparison Between Decentralized Local and Global Methods for Connectivity Maintenance of Multi-robot Networks. *IEEE Robotics and Automation Letters*, 4(2):633–640. <https://doi.org/10.1109/LRA.2019.2892552>.
- Lee, D., Franchi, A., Son, H. I., Ha, C., Bühlhoff, H. H., and Giordano, P. R. (2013). Semiautonomous Haptic Teleoperation Control Architecture of Multiple Unmanned Aerial Vehicles. *IEEE/ASME transactions on mechatronics*, 18(4):1334–1345. <https://doi.org/10.1109/TMECH.2013.2263963>.
- Park, H. and Hutchinson, S. (2018). Robust Rendezvous for Multi-robot System with Random Node Failures: An Optimization Approach. *Autonomous Robots*, 42(8):1807–1818. <https://doi.org/10.1007/s10514-018-9715-8>.
- Rizk, Y., Awad, M., and Tunstel, E. W. (2019). Cooperative Heterogeneous Multi-robot Systems: A Survey. *ACM Computing Surveys (CSUR)*, 52(2):1–31.
- Robuffo Giordano, P., Franchi, A., Secchi, C., and Bühlhoff, H. H. (2013). A Passivity-based Decentralized Strategy for Generalized Connectivity Maintenance. *The International Journal of Robotics Research*, 32(3):299–323. <https://doi.org/10.1177/0278364912469671>.
- Sabattini, L., Chopra, N., and Secchi, C. (2013). Decentralized Connectivity Maintenance for Cooperative Control of Mobile Robotic Systems. *The International Journal of Robotics Research*, 32(12):1411–1423. <https://doi.org/10.1177/0278364913499085>.
- Shah, S., Dey, D., Lovett, C., and Kapoor, A. (2018). Airsim: High-fidelity Visual and Physical Simulation for Autonomous Vehicles. In *Field and Service Robotics*, pages 621–635. Springer. [https://doi.org/10.1007/978-3-319-67361-5\\_40](https://doi.org/10.1007/978-3-319-67361-5_40).
- Shetty, A., Hussain, T., and Gao, G. (2021). Decentralized Connectivity Maintenance for Multi-robot Systems Under Motion and Sensing Uncertainties. In *Proceedings of the 34th International Technical Meeting of the Satellite Division of The Institute of Navigation (ION GNSS+ 2021)*.
- Shetty, A., Knowles, D., and Gao, G. X. (2020). Connectivity Maintenance for Multi-Robot Systems Under Motion and Sensing Uncertainties Using Distributed ADMM-based Trajectory Planning. *arXiv preprint arXiv:2012.09808*.

- Siligardi, L., Panerati, J., Kaufmann, M., Minelli, M., Ghedini, C., Beltrame, G., and Sabattini, L. (2019). Robust Area Coverage with Connectivity Maintenance. In *International Conference on Robotics and Automation (ICRA)*, pages 2202–2208. IEEE. <https://doi.org/10.1109/ICRA.2019.8793555>.
- Soukieh, R., Shames, I., and Fidan, B. (2009). Obstacle Avoidance of Robotic Formations Based on Fluid Mechanical Modeling. In *European Control Conference (ECC)*, pages 3263–3268. IEEE. <https://doi.org/10.23919/ECC.2009.7074908>.
- Yang, P., Freeman, R. A., Gordon, G. J., Lynch, K. M., Srinivasa, S. S., and Sukthankar, R. (2010). Decentralized Estimation and Control of Graph Connectivity for Mobile Sensor Networks. *Automatica*, 46(2):390–396. <https://doi.org/10.1016/j.automatica.2009.11.012>.